

# Statistical Analysis of Self-Organizing Networks with Biased Cell Association and Interference Avoidance

Carlos H. M. de Lima, *Member, IEEE*, Mehdi Bennis, *Member, IEEE*, and Matti  
Latva-aho, *Senior Member, IEEE*  
Email: {carlosl, bennis, matla}@ee.oulu.fi

## Abstract

In this work, we assess the viability of heterogeneous networks composed of legacy macrocells which are underlaid with self-organizing picocells. Aiming to improve coverage, cell-edge throughput and overall system capacity, self-organizing solutions, such as range expansion bias, almost blank subframe and distributed antenna systems are considered. Herein, stochastic geometry is used to model network deployments, while higher-order statistics through the cumulants concept is utilized to characterize the probability distribution of the received power and aggregate interference at the user of interest. A comprehensive analytical framework is introduced to evaluate the performance of such self-organizing networks in terms of outage probability and average channel capacity with respect to the tagged receiver. To conduct our studies, we consider a shadowed fading channel model incorporating log-normal shadowing and Nakagami- $m$  fading. Results show that the analytical framework matches well with numerical results obtained from Monte Carlo simulations. We also observed that by simply using almost blank subframes the aggregate interference at the tagged receiver is reduced by about 12dB. Although more elaborated interference control techniques such as, downlink bitmap and distributed antennas systems become needed, when the density of picocells in the underlaid tier gets high.

Authors are with the Centre for Wireless Communications (CWC), University of Oulu, Finland.

Authors would like to thank the Finnish funding agency for technology and innovation (Tekes), Elektrobit, Renesas Mobile, and Nokia Siemens Networks for supporting this work. This work has been also conducted in the framework of the ICT project ICT-4-248523 BeFEMTO, which is partly funded by the EU.

## I. INTRODUCTION

Targeting at upcoming releases, the 3<sup>rd</sup> Generation Partnership Project (3GPP) standardization body has focused on enhancing the end-user satisfaction and performance of Long Term Evolution (LTE) systems by adopting new deployments strategies and concepts such as Heterogeneous Networks (HetNets) and self-organization. In fact, legacy cellular systems with predefined structure and centralized coordination cannot keep up with the stringent requirements of next generation wireless systems, which demand high spectral efficiency and ubiquitous coverage with fairness at cell border. For instance, LTE-Advanced aims at peak data rates up to 1 Gbps which contrasts with current LTE systems which deliver at most 100 Mbps or even Asymmetric Digital Subscriber Line (ADSL) technology over copper landlines that can transmit at 24 Mbps only. Operators have indeed very few options available to meet such requirements: increase the density of macrocell sites, but that hinges on regulatory studies and approval; upgrade Radio Access Technology (RAT) which takes time and do not fill the capacity gap completely; or expand the radio spectrum resource, but that is definitely a very expensive and lingering alternative.

In this context, heterogeneous deployments which underlay legacy macrocells with low-cost, -power and -complexity small cells emerge as a promising and inexpensive alternative to meet these strict requirements. Future networks indeed benefit from self-organization in several situations, for example, to cope with the uncertainties of random networks wherein moving nodes need to communicate over volatile wireless channels; and to dynamically reconfigure and maintain infrastructureless deployments of small cells with large amount of nodes in which traditional and centralized methods become costly or even unfeasible. In order to tap into the full benefits of large-scale Self-Organizing Networks (SONs), a number of challenges still need to be tackled, including their deployment, operation, automation and maintenance [1], [2].

### A. Related Work

The design and implementation of self-organizing functionalities in HetNets is a topic of significant interest as evidenced by the number of recent publications [1], [3]–[8]. For instance, the self-organization concept is used to devise cognitive radio resource management schemes to mitigate cross-tier interference and guarantee users Quality of Service (QoS) in distinct heterogeneous deployments scenarios [9]. More recently, the Range Expansion Bias (REB) concept is discussed within 3GPP as a baseline solution to boost the offloading potential of heterogeneous deployments. In that regard, Authors in [10] investigate

the cell range expansion and interference mitigation in heterogeneous networks. Following the same lines, Güvenç instigates the capacity and fairness of heterogeneous networks with range expansion and interference coordination [4]. In [8], Jo *et al.* use the Stochastic Geometry (SG) framework to assess how the biased cell association procedure performs in heterogeneous networks by means of the outage probability. In multi-tier heterogeneous networks where the locations of Base Stations (BSs) are modeled as independent Poisson Point Process (PPP), the joint distribution of the downlink Signal-to-Interference plus Noise Ratio (SINR) at the tagged receiver is derived when the serving BS is selected as either the nearest or the strongest with respect to the user of interest [11].

### *B. Contributions and Organization*

In this work, we assess the performance of heterogeneous networks consisting of legacy macrocells with underlaid small cells. The offloading potential and self-organizing feature of small cells are studied so as to increase the overall spectral efficiency and meet the requirements of next generation systems as well. After providing definitions and models in Section II, a comprehensive analytical framework which resorts to SG and Higher Order Statistics (HOS) is then introduced to evaluate the performance of such heterogeneous deployments. We discuss the self-organizing solutions and network operation in Section IV. In that regard, we consider heterogeneous scenarios which employ REB to improve spatial reuse and balance load between tiers. To cope with the resulting Co-Channel Interference (CCI), Almost Blank Sub-frame (ABS) is considered as the baseline Inter-Cell Interference Coordination (ICIC) technique. Thereafter, a bitmap indicator, referred to as Downlink (DL)-High Interference Indicator (HII), is used to identify the dominant interferers and improve the Signal-to-Interference Ratio (SIR) at the receiver of interest. We then investigate the concept of virtual Distributed Antenna System (DAS) which is yet another self-organization solution to mitigate interference and improve the received signal at the receiver of interest. Afterwards, practical evaluation scenarios are defined in Section V wherein the resulting cross-tier interference and practical mechanism to mitigate it are of primary interest. Numerical results are provided in Section VI. Finally, we draw conclusions and make final remarks in Section VIII.

## II. SYSTEM MODEL AND ANALYTICAL FRAMEWORK

In preparation for the description of the evaluation scenarios and their performance analysis, we first present our assumptions, make definitions and introduce our system models.

### A. Definitions and Notation

**Definition 1: (Tagged receiver)** The Macrocell User (MU) who is taken as the reference to compute the aggregate CCI and performance metrics on the DL of the evaluation scenarios. In stochastic geometry, Palm distributions and the related Campbell's theorem are used to characterize a random pattern with respect to a typical point of the process, so that network-wide performance can be characterized by the average behavior of this "tagged" node [12], [13].

**Definition 2: (Observation region)** An annular region around the tagged receiver over which we account for the aggregate interference. The observation region is denoted by  $\mathcal{O}$  and defined by the minimum and maximum radii  $R_m$  and  $R_M$ , respectively.

**Definition 3: (Partial moment of a random variable)** Let  $Y$  be a Random Variable (RV), then  $E_Y^n[y_m, y_M] = \int_{y_m}^{y_M} y^n f_Y(y) dy$  denotes its  $n^{\text{th}}$  partial moment with  $y_m$  and  $y_M$  indicating the lower and upper integration limits, respectively.

### B. Propagation Channel Model

Radio links are degraded by path loss and shadowed fading, which is assumed to be independent over distinct network entities and positions. A signal strength decay function,  $l(r) = r^{-\alpha}$ , where  $\alpha$  is the path loss exponent, describes the path loss attenuation (unbounded path loss model [14]), while the received squared-envelop due to multi-path fading and shadowing is represented by a RV  $X \in \mathbb{R}^+$  with Cumulative Distribution Function (CDF) and Probability Density Function (PDF) denoted by  $F_X(x)$  and  $f_X(x)$ , respectively. An arbitrary interferer disrupts the communication of the tagged receiver with a component given by

$$Y = p l(r) x, \quad (1)$$

where  $p$  yields this interferer transmitted power,  $r$  is the separation distance from its position to the tagged receiver, and  $x$  yields the corresponding shadowed fading.

The composite distribution of the received squared-envelop due to Log-Normal (LN) shadowing and Nakagami- $m$  fading has a Gamma-LN distribution with PDF [15],

$$f_X(x) = \int_0^\infty \left(\frac{m}{\omega}\right)^m \frac{x^{m-1}}{\Gamma(m)} \exp\left(-\frac{m}{\omega}x\right) \times \frac{\xi}{\sqrt{2\pi\sigma\omega}} \exp\left[-\frac{(\xi \ln \omega - \mu_{\Omega_p})^2}{2\sigma_{\Omega_p}^2}\right] d\omega, \quad (2)$$

where  $m$  is the shape parameter of the Gamma distribution,  $\xi = \ln(10)/10$ ,  $\Omega_p$  is the mean squared-envelop,  $\mu_{\Omega_p}$  and  $\sigma_{\Omega_p}$  is the mean and standard deviation of  $\Omega_p$ , respectively.

Ho *et al.* show in [16] that a composite Gamma–LN distribution can be approximated by a single LN distribution with mean and variance (in logarithmic scale) given by  $\mu_{\text{dB}} = \xi [\psi(m) - \ln(m)] + \mu_{\Omega_p}$  and  $\sigma_{\text{dB}}^2 = \xi^2 \zeta(2, m) + \sigma_{\Omega_p}^2$ , where  $\psi(m)$  is the Euler psi function and  $\zeta(2, m)$  is the generalized Riemann zeta function [17]. In what follows, we use this single LN approximation to characterize the radio channel attenuations in various evaluation scenarios.

### C. Network Deployment Model

The DL of a heterogeneous networks consisting of an umbrella Macro Base Station (MBS) and an underlaid tier of self-organizing small cells is modeled. We assume that MBSs follow centralized coordination and spectrum allocation such that inter macrocell interference is mitigated, for example, using fractional frequency reuse [6]. In these scenarios, picocells are uniformly scattered over the network area, while both tiers operate in Time Division Duplexing (TDD) mode and share the whole spectrum. In addition, communicating nodes are assumed to be synchronized so that uplink and downlink transmissions do not interfere with each other. In every Sub-Frame (SF), each serving BS schedules a single user terminal and interference coordination are implemented in the time-domain. The set of associated user terminals are also uniformly distributed within the transmission range of their serving cells. Nodes communicate using antennas with omni directional radiation pattern and fixed power. The macrocell tier transmits at a maximum power of 46 dBm and picocells use 30 dBm.

Active picocells constitute a homogeneous PPP  $\Phi$  with density  $\lambda$  in  $\mathbb{R}^2$ . The number of picocells in an arbitrary region  $\mathcal{R}$  of area  $A$  is a Poisson RV with parameter  $\lambda A$  [18]. Additionally, we assume the fading effect as a random mark associated with each point of  $\Phi$ . By virtue of the Marking theorem [12], [18], the resulting process,

$$\tilde{\Phi} = \{(\varphi, x); \varphi \in \Phi\}, \quad (3)$$

corresponds to a Marked Point Process (MPP) on the product space  $\mathbb{R}^2 \times \mathbb{R}^+$ , whose random points  $\varphi$  denoting transmitters locations and belong to the stationary point process  $\Phi$ .

### D. Higher Order Statistics and the LN approximation

We introduce our analytical framework which uses stochastic geometry to model network deployments [18], [19], and higher order statistics through the cumulants concept to recover both the distributions of the received power  $Y$  and the aggregate CCI  $Z$  at the tagged receiver [17], [20]. The Slivnyak's theorem

and its associated Palm probability are then used to derive the aggregate CCI and compute average performance figures conditional on the location of the tagged receiver.

To establish this framework, we begin by applying Campbell's theorem [18], [19] to the MPP  $\tilde{\Phi}$  defined in (3) so as to determine the Characteristic Function (CF) of the distribution of the aggregate CCI.

*Definition 4:* Let  $Z = \sum_{(\varphi, x) \in \tilde{\Phi}} Y$  be a RV representing the aggregate CCI generated by the interfering process  $\tilde{\Phi}$ , and  $j = \sqrt{-1}$  be the imaginary unity; then, the function  $\Psi : \mathbb{R} \rightarrow \mathbb{C}$  defined as,

$$\Psi_Z(\omega) = \mathbb{E}[e^{j\omega Z}], \quad (4)$$

is called the CF of  $Z$ .

The corresponding  $n^{\text{th}}$  cumulants are obtained by computing higher order derivatives of (4) as presented in our next proposition [17].

*Proposition 1:* Let  $Z$  be a RV and  $\Psi_Z(\omega)$  its CF. Let  $n \in \mathbb{N}$ . Provided that the  $n^{\text{th}}$  moment exists and is finite. Then,  $\Psi_Z(\omega)$  is differentiable  $n$  times and

$$\kappa_n = \frac{1}{j^n} \left[ \frac{\partial^n}{\partial \omega^n} \ln \Psi_Z(\omega) \right]_{\omega=0} \quad (5)$$

*Proof:* See [21, Section 9.4]. ■

Motivated by the fact that the density of  $Z$  has no exact closed form expression [22] and that its distribution is heavy-tailed and positively skewed [20], we use the LN approximation whose parameters are estimated from the cumulants of the aggregate CCI. We relate the parameters of this equivalent LN distribution to the cumulants of the actual distribution of the aggregate CCI as follows,

$$\mu = \ln \left( \frac{\kappa_1^2}{\sqrt{\kappa_1^2 + \kappa_2}} \right), \text{ and } \sigma^2 = \ln \left( 1 + \frac{\kappa_2}{\kappa_1^2} \right). \quad (6)$$

where  $\mu$  is the mean and  $\sigma$  is the standard deviation of the distribution  $\text{Normal}(\mu, \sigma^2)$  in the logarithmic scale.

### III. BIASED CELL ASSOCIATION AND HANDOVER PROBABILITY

Following the standard handover procedure [23], the tagged MU is transferred to the underlaid picocell tier only if the pilot signal of the target Pico Base Station (PBS) is strictly higher than the umbrella MBS<sup>1</sup>

<sup>1</sup>We consider that migrating MUs are not affected by the ping-pong effect and that the predefined triggering time has already elapsed [24].

as follows,

$$Y^P > Y^M + \Omega, \quad (7)$$

where the RV  $Y^P$  refers to the power received from the target PBS,  $Y^M$  yields the power received from the umbrella MBS and  $\Omega$  is the handover hysteresis to avoid the ping-pong effect [24].

However, in most circumstances, the umbrella MBS overpowers the underlaid tier which shrinks the coverage of the small cells and compromises the expected gains of spatial and frequency reuse [4], [10]. In such large-scale heterogeneous deployments, transceivers have various communication capabilities and the restrictive nature of the typical handover procedure worsen the load unbalance problem across tiers. To alleviate this problem, 3GPP suggests adding a positive bias  $\Delta\text{REB}$  to the picocells received power so that the rate of MUs handovers to the underlaid tier increases [10] as given next

$$Y^P + \Delta\text{REB} > Y^M + \Omega. \quad (8)$$

Indeed, the REB prompt the macrocell offloading and improves the spectral efficiency by relaxing the standard association criteria used by MUs. Unfortunately, by doing so, MUs within the expanded region of picocells do not actually connect to the strongest BSs and are exposed to high interference levels from the macrocell tier. Fig. 1 illustrates the operation of the REB concept in heterogeneous scenarios composed of an umbrella macrocell and underlaid picocells. The coverage area of the target picocell is artificially increased by the positive bias  $\Delta\text{REB}$  as indicated by the handover criterion in (8). As a result, MUs are offloaded to the picocell tier more often and unburden the umbrella macrocell.

From (8), we derive the probability that the tagged MU within the coverage of the umbrella MBS is offloaded to the target PBS. The LN approximation in (6) is used here to recover the distribution of the received power at the tagged receiver.

*Proposition 2:* Consider the observation region  $\mathcal{O}$  centered at the tagged receiver and the biased cell association as described above; then, the probability that the tagged receiver connects to the target PBS is given by,

$$\Pr[Y^M < Y^P + \delta] \simeq \sum_{k=1}^K \frac{\omega_k}{2\sqrt{\pi}} g(\eta_k), \quad (9)$$

where  $\delta = \Delta\text{REB} - \Omega$ ,  $\eta_k$  is the  $k^{\text{th}}$  zero of the Hermite polynomial  $H_K(\eta)$  of degree  $K$ ,  $\omega_k$  is the corresponding weight of the function  $g(\cdot)$  at the  $k^{\text{th}}$  abscissa and  $g(\eta) = 1 + \text{Erf}\left[\frac{-\mu_M + \mu_P + \sqrt{2}\eta\sigma_P}{\sqrt{2}\sigma_M}\right]$ .

*Proof:* See Appendix A. ■

When using the standard procedure in (7), one needs to make the substitution  $\delta = -\Omega$  in (9) to derive the handover probability.

Fig. 2 shows the handover probability for distinct network configurations. To generate this plot, we consider that the tagged receiver is randomly placed around the umbrella MBS in an annular region with inner radius equal to 25 m and outer radius of either 250 m or 500 m. Notice that this region actually defines the minimum and maximum distances between the tagged receiver and the umbrella MBS. In addition, the distance from the tagged receiver to its serving picocell varies within the set  $\{15, 30, 45\}$  m. When the MU is near to the target picocell, the REB does not affect the handover probability so significantly. However, the REB effect becomes pronounced when the user is located farther away from the picocell of interest. For sake of illustration, we consider the tagged user located 45 m away from the target picocell and bias of  $\Delta\text{REB} = 5$  dB. In contrast to the standard approach in (7), the handover probability increases from 38% to 54% (dashed line with up-triangles).

#### IV. NETWORK OPERATION

In the coexistence scenarios under study, self-organizing PBSs employ distributed strategies to control the cross-tier interference [1]. Hereafter, we describe these solutions and translate their operation to our mathematical framework so as to identify their impact on the overall system performance.

##### A. Almost Blank Sub-frame

By observing Fig. 1, it is clear that within the range expanded region the received power of the target picocell with REB is weaker than the umbrella MBS. To cope with this problem in such SON, the ABS is considered as a baseline strategy to implement interference control. In fact, ABS is a time-domain resource partitioning strategy whereby MUs in the expanded region of picocells only transmit within the reserved slots. During these reserved slots, the umbrella MBS either implements soft ABS by transmitting with less power; or does not transmit at all what characterizes the zero-power ABS [25]. In Fig. 3, the aggressor MBS does not transmit during the reserved slots so as to protect the range expanded picocells. We follow [10] in assuming that only cells with REB are allowed to transmit within the reserved subframes. The downside of the ABS strategy is that non-REB cells undergo capacity loss since reserved subframes are left idle. Different from the typical approach and depending on the network configuration, we consider that ABS applies to both macro and picocells. There is no loss of generality



in assuming that the umbrella MBS reserves 1/2 of the frame for the ABS allocation [6] when operating with REB.

### B. Downlink–High Interference Indicator

To avoid the inherent capacity loss of the ABS strategy, we also investigate distributed strategies that rely on the autonomous coordination of nearby BSs. Inspired by the busy tones concept [26] and the interference mitigation technique in [27], we consider the utilization of DL channel measurements for the coordination of interfering picocells. A bitmap indicator which is similar to the Relative Narrowband Transmit Power (RNTP) indicator in Release 8 is used to identify dominant interferers [28]. The tagged MU identifies potential interferers by monitoring their pilot signal and reporting the measurements to its serving BS. After acquiring this measurement report, the serving BS then coordinates by exchanging the interference bitmap with the surrounding picocells via the X2 interface. The updating period of the DL-HII messages is a configurable parameter which is comparable to the handover procedure [29].

Within our mathematical framework, the tagged receiver uses the interference threshold  $\rho_{th}$  to identify potential interferers in its vicinity. Since our network operates in TDD mode, we assume that the channels for measurements and data transmissions are fully correlated. Furthermore, the channel gain between active interferers and the tagged receiver are assumed to be perfectly estimated by the receiver of interest.

Under the above assumptions, the set of dominant interferers is identified by the following indicator function,

$$\mathbf{1}_{\tilde{\Phi}}(p_b r^{-\alpha} x) = \begin{cases} 1, & \text{if } p_b r^{-\alpha} x \geq \rho_{th} \\ 0, & \text{otherwise,} \end{cases} \quad (10)$$

which defines the first coordination region denoted by  $\mathcal{R}_1$ , and where  $p_b$  is the transmit power of the reference signal of surrounding picocells.

In accordance with the formulation of Section II-C, picocells within this region constitute a MPP which is denoted by  $\tilde{\Phi}_1 = \{(\varphi, x) \in \tilde{\Phi} \mid p_b r^{-\alpha} x \geq \rho_{th}\}$ . Similarly, picocells in  $\mathcal{R}_2$ , which are not detected by the MU of interest, form the process  $\tilde{\Phi}_2 = \tilde{\Phi} \setminus \tilde{\Phi}_1$ . Notice that the coordination regions  $\mathcal{R}_1$  and  $\mathcal{R}_2$  are disjoint and statistically independent by construction, therefore it follows immediately from the Superposition theorem [18] that  $\tilde{\Phi} = \tilde{\Phi}_1 \cup \tilde{\Phi}_2$ . Fig. 4 illustrates the resulting coordination regions by following the criterion in (10). It is worth noticing that after coordinating, the tagged receiver is only interfered by active transmitters in  $\mathcal{R}_2$ , since nodes in  $\mathcal{R}_1$  switch to non-conflicting resource allocation.

### C. Virtual Distributed Antenna System

By following the standard REB strategy, a user is served by a BS which does not actually provide the strongest received power which brings about the side effect of exposing the user of interest to high interference levels. With the virtual DAS strategy, we intend to further exploit the HII bitmap information so that surrounding picocells coordinate over the X2 interface and establish virtual DAS with random antenna layout. As discussed in [30], such techniques are actually a work item in the 3GPP standardization where large scale remote radio heads are seen as a promising solution to meet the requirements of release 11. Note that with this solution we do not consider Transmit Antenna Selection (TAS) or precoding and the received signals of the serving DAS coherently add at the user of interest. Instead of considering the REB, the tagged MU uses the aggregate received power from the serving group which belongs to  $\tilde{\Phi}_1$ . Similar to the coordinated multipoints strategy, this solution requires the user data to be available at all coordinating picocells which in its turn requires extra signaling exchange and more elaborated backhaul infrastructure [31]. Our strategy is similar to the maximum ratio transmission [32] by which all antenna elements transmit the same information and the aggregate received power is

$$\sum_{(\varphi, x) \in \tilde{\Phi}_1} Y^P(\varphi, x) \quad (11)$$

where  $Y^P(\varphi, x)$  yields the received power from the picocell at  $\varphi$  with shadowed fading  $x$ . It is worth noticing that the random process  $\tilde{\Phi}_1$  has intensity given by  $\Pr [p_b r^{-\alpha} x \geq \rho_{\text{th}}] \lambda f_X(x)$ .

In what follows, we initially extend the analytical framework presented in [33] to evaluate how these distributed strategies perform in heterogeneous networks composed of self-organizing small cells and legacy macrocells. Thereafter, the performance of the SON is evaluated in terms of SIR, outage probability and average spectral efficiency as shown in Section VI.

## V. INTERFERENCE MODEL

Under the assumptions of Section II and with respect to the tagged receiver, we now use our analytical framework to derive the probability distributions of the desired signal and the resulting aggregate CCI for each one of the Evaluation Scenarios (ESs) described next. In fact, each ES characterizes a particular network configuration, in which macro and picocells employ distributed strategies to mitigate the cross-tier interference. The following list summarizes the evaluation scenarios under consideration.

- ES1: the tagged MU connects to the umbrella MBS and experiences full interference from the underlaid picocell tier.

- ES2: the tagged MU connects to the target PBS with REB, but no ICIC strategy, such as ABS, is carried out. As a result, the user of interest which dwells in the Range Expansion (RE) region of the serving picocell is subject to high interference levels from the umbrella macrocell.
- ES3: the tagged MU connects to the target PBS with REB, and the umbrella MBS implements the ABS scheme with rate 1/2.
- ES4: the tagged MU connects to the target PBS, and the surrounding picocells coordinate based on the DL-HII bitmap [29], although the umbrella MBS still interferes. This configuration is particularly relevant when the density of small cells nearby the tagged receiver is high, or there are multiple tiers of interfering small cells, such as femtocells.
- ES5: based on the DL-HII bitmap, the strongest picocells coordinate so as to implement a virtual DAS. However, the umbrella MBS and small cells in  $\mathcal{R}_2$  still interfere with the user of interest. It is assumed that the picocells coordinate through the X2 interface. However, picocells can also coordinate over the air interface for example using the coordination mechanism introduced in [33].

#### A. Received Power from the Umbrella MBS

In this section, we initially derive the CF [17], [20], [34] of the RV which describes the power received from a random transmitter within  $\mathcal{O}$  and thereafter particularize it to the umbrella MBS case. By considering the communication model of Section II-C, we write the CF of the power received at the tagged MU from a random transmitter within its observation region as follows.

*Proposition 3:* Let  $Y = R^{-\alpha}X$  be a RV describing the power received at the tagged receiver from a random transmitter in  $\mathcal{O}$  with  $R$  varying from  $R_m$  to  $R_M$  and  $X$  following the Gamma-LN distribution of Section II. Then, the CF of  $Y$  is

$$\Psi_Y(\omega) = \frac{2}{R_M^2 - R_m^2} E_X [R(\omega)], \quad (12)$$

where  $R(\omega) = \int_{R_m}^{R_M} \exp(j\omega p r^{-\alpha} x) r dr$  and  $E_X[\cdot]$  yields the expectation of the enclosed expression over the RV  $X$ .

*Proof:* See Appendix B. ■

It is worthy noting that (12) is a general formulation which characterizes the distribution of any random transmitter within the reception range of the tagged receiver including the umbrella MBSs and small cells in the underlaid tier.

Thereafter, by taking the  $n^{\text{th}}$  derivative of the CF as given in (5), the corresponding cumulant  $\kappa_n$  is obtained.

*Proposition 4:* Consider the CF of the power received from a transmitter randomly deployed within the observation region  $\mathcal{O}$ ; then, the  $n^{\text{th}}$  cumulant of  $Y$  is given by

$$\kappa_n = \frac{1}{j^n} \sum_{k=0}^n g^{(k)}(\beta_0) \cdot B_{n,k}[\beta_1, \beta_2, \dots, \beta_{(n-k+1)}], \quad (13)$$

where  $g(u) = \ln(u)$ ,  $B_{n,k}[\beta_1, \beta_2, \dots, \beta_{(n-k+1)}]$  is the partial Bell polynomial [35] and  $\beta_n = j^n p^n \times \frac{R_m^{2-n\alpha} - R_M^{2-n\alpha}}{n\alpha - 2} \mathbb{E}_X[x^n]$ .

*Proof:* See Appendix C. ■

### B. Aggregate CCI from the Underlaid Tier of Small Cells

This scenario represents our default configuration in which the umbrella MBS serves the tagged receiver, whereas the underlaid picocell tier is the only source of interference. In order to characterize the distribution of the aggregate CCI at the tagged receiver, we use the cumulant-based framework with the MPP  $\tilde{\Phi}$  [20], [33]. By applying Campbell's theorem to (3), we derive its characteristic functional [18] as given next.

*Proposition 5:* Consider the ES1; then, the  $n^{\text{th}}$  cumulant of the aggregate CCI perceived by the tagged MU within  $\mathcal{O}$  and with respect to  $\tilde{\Phi}$  is given by,

$$\kappa_n(\tilde{\Phi}) = \frac{2\pi\lambda p^n}{n\alpha - 2} (R_m^{2-\alpha n} - R_M^{2-\alpha n}) \mathbb{E}_X^n[0, \infty]. \quad (14)$$

*Proof:* See Appendix D. ■

The aggregate CCI from the underlaid tier of picocells is computed with respect to a limited region of the total field of interfering nodes (from  $R_m$  to  $R_M$ ). To account for the neglected interference parcel beyond  $R_M$ , one needs to change in (32) the upper limit of integration with respect to  $r$  until  $\infty$ . For instance, considering  $\alpha = 3$ ,  $R_m = 5\text{m}$  and  $R_M = 250\text{m}$ , the aggregate interference from the region beyond  $R_M = 250\text{m}$  (towards  $\infty$ ) represents only 2% of the aggregate interference, whereas for an observation region within  $R_m = 25\text{m}$  and  $R_M = 500\text{m}$  the neglected region contributes with 5% of the total interference.

### C. Aggregate CCI from Multiple Tiers

The additivity property of cumulants is used to compute the aggregate CCI in heterogeneous scenarios with multiple tiers [36]. In order to apply this property, the interference components are assumed to be independent.

*Proposition 6:* Consider the two tier deployment scenario where an umbrella MBS is underlaid with self-organizing small cells; then, the  $n^{\text{th}}$  cumulant of the aggregate CCI perceived by the tagged MU in  $\mathcal{O}$  is,

$$\kappa_n = \kappa_n^{\text{M}} + \kappa_n^{\text{P}}. \quad (15)$$

*Proof:* Since the interference components from both tiers are independent of each other, we can use the cumulants additivity property to obtain (15). ■

### D. Aggregate CCI with Inter-Cell Interference Coordination

As shown in Section IV-B, picocells use the DL-HII bitmap to self-organize into two coordination regions  $\mathcal{R}_1$  and  $\mathcal{R}_2$ . Herein, we derive the cumulants of the aggregate CCI generated by each such region with respect to the tagged receiver. Small cells that are detected by the tagged receiver within  $\mathcal{R}_1$  decrease their transmit power by a predefined value, *i.e.*,  $p' = p - \Delta p$  so as to reduce their interference towards the user of interest. In the following proposition, the cumulants of the dominant interfering picocells belonging to MPP  $\tilde{\Phi}_1$  are identified.

*Proposition 7:* Consider the network operation of Section IV-B; then, the  $n^{\text{th}}$  cumulant of the aggregate CCI perceived by the tagged MU in  $\mathcal{O}$  with respect to  $\tilde{\Phi}_1$  is written as,

$$\begin{aligned} \kappa_n(\tilde{\Phi}_1) = & \frac{2\pi\lambda(p')^n}{n\alpha - 2} \left\{ (R_m^{2-\alpha n} - R_M^{2-\alpha n}) \text{E}_X^n[\varrho_M, \infty] - \varrho_{th}^{n-\frac{2}{\alpha}} \text{E}_X^{\frac{2}{\alpha}}[\varrho_m, \varrho_M] \right. \\ & \left. + R_m^{2-n\alpha} \text{E}_X^n[\varrho_m, \varrho_M] \right\}. \end{aligned} \quad (16)$$

*Proof:* See Appendix E. ■

During the coordination mechanism, the tagged receiver does not detect the picocells within  $\mathcal{R}_2$  which contribute to the aggregate interference with transmit power  $p$  dBm. Therefore, the distribution of the remaining interference is characterized by the following cumulants.

*Proposition 8:* Consider the network operation of Section IV-B; then, the  $n^{\text{th}}$  cumulant of the aggregate CCI perceived by the tagged MU in  $\mathcal{O}$  with respect to  $\tilde{\Phi}_2$  has the following form,

$$\begin{aligned} \kappa_n(\tilde{\Phi}_2) = \frac{2\pi\lambda p^n}{n\alpha - 2} & \left\{ (R_m^{2-\alpha n} - R_M^{2-\alpha n}) \mathbb{E}_X^n[-\infty, \varrho_m] + \varrho_{th}^{n-\frac{2}{\alpha}} \mathbb{E}_X^{\frac{2}{\alpha}}[\varrho_m, \varrho_M] \right. \\ & \left. - R_M^{2-n\alpha} \mathbb{E}_X^n[\varrho_m, \varrho_M] \right\}. \end{aligned} \quad (17)$$

*Proof:* See Appendix F. ■

## VI. PERFORMANCE ANALYSIS

With regard to the tagged receiver, the performance of the evaluation scenarios is assessed by means of the resulting outage probability and average channel capacity. The scenarios under study are interference limited and hence the thermal noise is negligible in comparison to the resulting CCI [37].

### A. SIR and Outage Probability

The outage probability is given by  $\Pr[\Gamma < \gamma_{\text{th}}]$  where the RV  $\Gamma$  represents the SIR distribution of the tagged receiver, and  $\gamma_{\text{th}}$  is the corresponding SIR detection threshold.

*Theorem 1:* Let  $V_0$  and  $V$  be Normal RVs (in logarithmic scale) representing the power received from the desired transmitter and the aggregate CCI at the tagged receiver, respectively. Under the assumption of the shadowed fading with composite Gamma-LN distribution, the SIR at the tagged receiver is

$$\Gamma \sim \text{Normal}(\mu_{V_0} - \mu_V, \sigma_{V_0}^2 + \sigma_V^2), \quad (18)$$

and the outage probability is given by

$$\Pr[\Gamma < \gamma_{\text{th}}] = \mathbb{Q}[(\mu_\Gamma - \gamma_{\text{th}})/\sigma_\Gamma], \quad (19)$$

where  $\mu_\Gamma = \mu_{V_0} - \mu_V$  and  $\sigma_\Gamma = \sqrt{\sigma_{V_0}^2 + \sigma_V^2}$ .

*Proof:* The SIR distribution is given by the quotient of two independent LN RVs, namely,  $e^{V_0}$  which is the received power from the target transmitter, and  $e^V$  which is an equivalent LN RV approximating the aggregate CCI at the tagged receiver. Hence, the multiplicative reproductive property of LN RVs is applied to obtain the SIR distribution [34]. ■

### B. Average Spectral Efficiency

We evaluate how the two-tier coexistence scenarios perform in terms of the location-dependent average channel capacity of the tagged receiver [38]. By using the analytical framework previously established, and assuming that all users are allocated on the same bandwidth  $W$ , we initially recover the SIR distribution of the tagged receiver, and then compute the corresponding capacity.

*Theorem 2:* Under the assumption of the shadowed fading channel regime, the average channel capacity of the tagged receiver is given as,

$$\bar{C} \simeq W \sum_{k=1}^K \frac{\omega_k}{\sqrt{\pi}} \log_2 \left[ 1 + \exp \left( \frac{\eta_k \sqrt{2}\sigma + \mu}{\xi} \right) \right]. \quad (20)$$

*Proof:* To compute the location-dependent average channel capacity,

$$\bar{C} = W \int_0^{\infty} \log_2 (1 + \gamma) f_{\Gamma}(\gamma) d\gamma, \quad (21)$$

we use the PDF of the SIR with respect to the tagged receiver, which is indicated by  $f_{\Gamma}(\gamma)$ . The Gauss-Hermite quadrature [17] with the substitution  $\eta = (\xi \ln \gamma - \mu)/\sqrt{2}\sigma$  are used to obtain (20). ■

As discussed in [7], [39] the aggregate interference perceived by the tagged receiver has non-Gaussian nature, and the Shannon formula is used as a lower bound for the ergodic rate.

## VII. NUMERICAL RESULTS

By using the analytical framework of Section II-D, the distributions of the received power, aggregate CCI and the resulting SIR are calculated for each one the ESs. The outage probability and average channel capacity are also used to evaluate how the system performs with biased cell association and interference coordination techniques.

Fig. 5 compares the CDF of the picocell received power at the tagged receiver ( $Y^P$ ) from Monte Carlo simulations with those obtained with the LN approximation. In this example, the annular observation region is defined by  $R_m = 5$  m and  $R_M = 75$  m and picocells operate with a fixed power level of 30 dBm. The radio channel is affected by path loss with exponent  $\alpha = 3$ , LN shadowing with standard deviation  $\sigma = 6, 8, 10$  and 12 dB, and Nakagami fading with shape parameter  $m = 16$  which corresponds to a Rician channel with parameter  $K = 14.8$  dB. The proposed framework approximates well the power received by the tagged receiver from a random picocell within its observation region for varying number of interfering scenarios. Similarly, Fig. 6 shows the CDF of the distribution of the power received from

the umbrella macrocell at the tagged receiver ( $Y^M$ ). The umbrella MBS transmits at 43 dBm. As can be seen, our LN model matches well the simulation results in the macrocell configuration. In addition, the LN approximation is tighter for larger  $\sigma$  (standard deviation), when the resulting shadowing dominates the variation of the received power distribution.

Fig. 7 compares the Complementary Cumulative Distribution Function (CCDF) of the aggregate CCI from Monte Carlo simulations with those from the proposed LN approximation. Our approximation matches well with the simulation results for the evaluation scenarios under study. An annular observation region with  $R_m = 25$  m and  $R_M = 250$  m is considered. Picocells operate with a fixed power level of 30 dBm and constitute a Poisson field of interferers with intensity  $\lambda = 10^{-5}$  PBS/m<sup>2</sup> (about 2 picocells on average). By comparing the scenario where PBSs are the only source of interference with that in which PBSs and the umbrella MBS jointly interfere, it is possible to identify the harmful impact of the macrocell component at the tagged receiver (about 12 dB). With that effect in mind, the benefits of using ABS to avoid the interference from the umbrella macrocell altogether becomes evident. Afterwards, we increase the density of picocells to  $\lambda = 10^{-4}$  PBS/m<sup>2</sup> (about 20 cells on average) and allow surrounding picocells to use the downlink HII in order to coordinate with the serving BS. As a result, the interference experienced by the tagged receiver is further reduced. An interesting observation is that depending on the density of picocells and their relative distance to the tagged receiver, the underlay picocell tier dominates the aggregate interference.

Fig. 8 shows the outage probability for distinct evaluation scenarios and increasing density of PBSs. The expressions (18) and (19) in Theorem 1 are used to generate the numerical results shown in this figure. By comparing the outage probability of the tagged receiver in ES2 and ES3, one observes a performance improvement by avoiding the interference from the umbrella MBSs, which is the dominant interferer. However, the underlaid tier of picocells dominates the resulting interference as the density of picocells increases – The ABS gains are not so evident for a density  $\lambda$  higher than  $7 \times 10^{-5}$  PBS/m<sup>2</sup>. Hence, the coordination mechanisms are considered in this work to further reduce the interference levels at the tagged receiver. When interfering picocells coordinate their transmissions by fulfilling the criterion  $\mathbb{1}_{\tilde{\Phi}}(p_b r^{-\alpha} x)$  in scenarios ES4 and ES5, the network operation outperforms the standard configuration wherein BSs do not self-organize. In fact, when nodes coordinate following the criterion given in (10), the tagged receiver experiences much better link quality since less interferers are active in its reserved subframes.



In Fig. 9, we use (20) (see Theorem 2) to compute the average channel capacity of the tagged link for an increasing density of interfering picocells. The performance of the tagged receiver is severely degraded by the umbrella MBS which corroborates our previous outage probability results. By employing interference avoidance techniques in scenarios ES4 and ES5, the channel capacity of the tagged receiver link improves significantly. In addition, the tagged receiver benefits mostly from the coordination of surrounding picocells by means of the DL-HII which corresponds to ES4 and ES5. For instance, the tagged receiver attains at most 1bps/Hz in ES3, while an average channel capacity of about 2.5bps/Hz is achieved in ES5.

### VIII. CONCLUSIONS AND FINAL REMARKS

In this paper, we investigate the problem of co-channel interference in heterogeneous networks composed of self-organizing small cells and legacy macrocells. An analytical framework which resorts to stochastic geometry and higher-order statistics through the concept of cumulants is introduced in order to characterize network dynamics and channel variations. We use this framework to recover the distribution of the CCI and to evaluate the system performance in terms of outage probability and average spectral efficiency of the tagged link. For the scenarios under study, results show that our analytical model matches well with numerical results obtained using Monte Carlo simulations. Aiming to reduce the co-channel interference generated at the underlaid tier, picocells coordinate their transmissions using the DL-HII incurring minimum overhead. Finally, by employing the concept of virtual DASs, the user of interest not only benefits from reduced interference, but also from the maximum ratio transmission among the serving picocells.

#### APPENDIX A

##### PROOF OF PROPOSITION 2

From (6), we know that  $Y^M$  and  $Y^P$  follow LN distribution with parameters  $(\mu_M, \sigma_M)$  and  $(\mu_P, \sigma_P)$ , respectively. Thus, the handover probability is given by

$$\Pr [Y^M < Y^P + \delta] = \int_0^{\infty} \int_0^{y^P + \delta} f_{Y^M}(y^M) f_{Y^P}(y^P) dy^M dy^P. \quad (22)$$

where  $f_{Y^M}(y^M)$  and  $f_{Y^P}(y^P)$  yield the probability density function of the umbrella MBS and target picocell, respectively. After evaluating the inner-most integral, we obtain

$$\Pr[Y^M < Y^P + \delta] = \int_0^\infty \frac{1}{2} \operatorname{Erfc} \left[ \frac{\mu_M - \log(c + y^P)}{\sqrt{2}\sigma_M} \right] f_{Y^P}(y^P) dy^P \quad (23)$$

After making the change of variate  $\eta = \frac{-\mu_P + \log(y^P)}{\sqrt{2}\sigma_P}$  in (23), we obtain

$$\Pr[Y^M < Y^P + \delta] = \int_{-\infty}^{\infty} \frac{e^{-\eta^2} \operatorname{Erfc} \left[ \frac{\mu_M - \log(c + e^{\mu_P + \sqrt{2}\eta\sigma_P})}{\sqrt{2}\sigma_M} \right]}{2\sqrt{\pi}} d\eta \quad (24)$$

To evaluate  $\Pr[Y^M < Y^P + \delta]$  in (24), we then use the Gauss-Hermite quadrature [17],

$$\int_{-\infty}^{+\infty} e^{-\eta^2} f(\eta) d\eta = \sum_{k=1}^K \omega_k f(\eta_k) + R_K, \quad (25)$$

where  $\eta_k$  is the  $k^{\text{th}}$  zero of the Hermite polynomial  $H_K(\eta)$  of degree  $K$ ,  $\omega_k$  is the corresponding weight of the function  $f(\cdot)$  at the  $k^{\text{th}}$  abscissa, and  $R_K$  is the remainder value. Finally, we obtain (9) by performing the substitutions indicated above.

## APPENDIX B

### PROOF OF PROPOSITION 3

From (1), the CF of the representative interference component of a random transmitter within the observation region  $\mathcal{O}$  is written as,

$$\begin{aligned} \Psi_Y(\omega) &= \mathbb{E}[e^{j\omega Y}] \\ &= \int_0^\infty \int_{R_m}^{R_M} e^{j\omega pr^{-\alpha} x} f_{R,X}(r, x) dr dx. \end{aligned} \quad (26)$$

where  $f_{R,X}(r, x)$  is the joint density function of the separation distance between interferers and the tagged receiver, and the shadowed fading. Recalling that the finite field of interferers is within an observation region which is delimited by  $R_m$  and  $R_M$ , the PDF of the distances from random points uniformly scattered within  $\mathcal{O}$  to the tagged receiver is,

$$f_R(r) = \frac{2r}{R_M^2 - R_m^2}. \quad (27)$$

By substituting (27) in (26), we obtain

$$\Psi_Z(\omega) = \frac{2}{R_M^2 - R_m^2} \int_0^\infty \int_{R_m}^{R_M} \exp(j\omega pr^{-\alpha}x) f_X(x) r dr dx. \quad (28)$$

After manipulating the above expression by performing substitutions and simplifications as indicated in Proposition 3, we obtain (12).

## APPENDIX C

### PROOF OF PROPOSITION 4

Consider the auxiliary functions  $f(\omega) = \int_0^\infty \int_{R_m}^{R_M} \exp(j\omega pr^{-\alpha}x) f_X(x) r dr dx$  and  $(g \circ f)(\omega) = \ln[f(\omega)]$ . Now, using the Faà di Bruno's formula [17] which generalizes the chain rule to compute higher order derivatives of the composition of two functions  $(g \circ f)(\omega)$ , we have

$$\frac{\partial^n}{\partial \omega^n} (g \circ f)(\omega) = \sum_{i=0}^n g^{(i)}[f(\omega)] \cdot B_{n,i}[f'(\omega), f''(\omega), \dots, f^{(n-i+1)}(\omega)], \quad (29)$$

where  $B_{n,i}[f'(0), f''(0), \dots, f^{(n-i+1)}(0)]$  is the partial Bell polynomial [35]. After evaluating (29) at  $\omega = 0$  and using the definition of cumulants from (5), we obtain the following result

$$\kappa_n = \frac{1}{j^n} \sum_{i=0}^n g^{(i)}[f(0)] \cdot B_{n,i}[f'(0), f''(0), \dots, f^{(n-i+1)}(0)]. \quad (30)$$

The derivatives of the auxiliary function  $f(\omega)$  at zero are given by,

$$\begin{aligned} \beta_n &= \left. \frac{\partial^n f(\omega)}{\partial \omega^n} \right|_{\omega=0} \\ &= j^n p^n \int_0^\infty x^n f_X(x) dx \int_{R_m}^{R_M} r^{1-n\alpha} dr. \end{aligned} \quad (31)$$

By substituting (31) into (30), the final expression for the  $n^{\text{th}}$  cumulant of the aggregate CCI in (13) results.

## APPENDIX D

### PROOF OF PROPOSITION 5

We start from (4) and apply Campbell's theorem [18], [19] to derive the CF of the aggregate CCI perceived by the tagged MU as

$$\Psi_Z(\omega) = \exp \left\{ 2\pi \int_0^\infty \int_{R_m}^{R_M} \left[ \exp(j\omega pr^{-\alpha}x) - 1 \right] \lambda f_X(x) r dr dx \right\}. \quad (32)$$

By substituting (32) in (5), and after integrating with respect to  $r$ , we write the  $n^{\text{th}}$  cumulant as

$$\kappa_n(\tilde{\Phi}) = \frac{2\pi\lambda p^n}{n\alpha - 2} (R_m^{2-\alpha n} - R_M^{2-\alpha n}) \int_0^\infty x^n f_X(x) dx. \quad (33)$$

Recalling that  $E_X^n[0, \infty] = \int_0^\infty x^n f_X(x) dx$ , we turn our attention to the case where transmissions are affected by the shadowed fading, and so from Section II-B,  $E_X^n[0, \infty] = e^{n\mu + \frac{1}{2}n^2\sigma^2}$  which gives (14).

## APPENDIX E

### PROOF OF PROPOSITION 7

By using the indicator function in (10), we write the CF of the aggregate CCI for the  $\mathcal{R}_1$  as,

$$\Psi_{Z_1}(\omega) = \exp \left\{ 2\pi \int_0^\infty \int_{R_m}^{R_M} \left[ \exp(j\omega p' r^{-\alpha} x) - 1 \right] \lambda f_X(x) \mathbf{1}_{\tilde{\Phi}}(p_b r^{-\alpha} x) r dr dx \right\}. \quad (34)$$

And from (5) the  $n^{\text{th}}$  cumulant is,

$$\begin{aligned} \kappa_n &= 2\pi\lambda \int_X \int_{R_m}^{\min[R_M, (x/\varrho_{th})^{1/\alpha}]} (p')^n r^{1-n\alpha} x^n f_X(x) dr dx \\ &= 2\pi\lambda \left[ \int_{\varrho_M}^\infty \int_{R_m}^{R_M} (p')^n r^{1-n\alpha} x^n f_X(x) dr dx + \int_{\varrho_m}^{\varrho_M} \int_{R_m}^{(x/\varrho_{th})^{1/\alpha}} (p')^n r^{1-n\alpha} x^n f_X(x) dr dx \right], \end{aligned} \quad (35)$$

where  $\varrho_m = \varrho_{th} R_m^\alpha$  and  $\varrho_M = \varrho_{th} R_M^\alpha$ . By integrating (35) with respect to  $r$ , we obtain

$$\kappa_n = \frac{2\pi\lambda (p')^n}{n\alpha - 2} \left\{ (R_m^{2-\alpha n} - R_M^{2-\alpha n}) \int_{\varrho_M}^\infty x^n f_X(x) dx + \int_{\varrho_m}^{\varrho_M} \left[ x^n R_m^{2-n\alpha} - x^{\frac{2}{\alpha}} \varrho_{th}^{n-\frac{2}{\alpha}} \right] f_X(x) dx \right\}. \quad (36)$$

Finally, we compute the partial moments of the approximating LN RV  $X$  by repeatedly applying Definition 3, and by using the change of variable  $X = e^{\mu + \sigma Z}$ , where  $Z \sim \text{Normal}(0, 1)$ , along with the substitutions  $\tilde{\varrho}_M = \frac{\ln \varrho_M - \mu}{\sigma}$  and  $\tilde{\varrho}_m = \frac{\ln \varrho_m - \mu}{\sigma}$ .

$$E_X^n[\varrho_M, \infty] = e^{n\mu + \frac{n^2\sigma^2}{2}} Q[\tilde{\varrho}_M - n\sigma], \quad (37)$$

$$E_X^{\frac{2}{\alpha}}[\varrho_m, \varrho_M] = e^{\frac{2\mu}{\alpha} + \frac{2\sigma^2}{\alpha^2}} \left( Q\left[\tilde{\varrho}_m - \frac{2\sigma}{\alpha}\right] - Q\left[\tilde{\varrho}_M - \frac{2\sigma}{\alpha}\right] \right), \quad (38)$$

$$E_X^n[\varrho_m, \varrho_M] = e^{n\mu + \frac{n^2\sigma^2}{2}} (Q[\tilde{\varrho}_m - n\sigma] - Q[\tilde{\varrho}_M - n\sigma]), \quad (39)$$

where  $Q[u] = \frac{1}{\sqrt{2\pi}} \int_u^\infty e^{-\frac{v^2}{2}} dv$ . And by replacing the above expressions in (35), (16) results.

APPENDIX F  
PROOF OF PROPOSITION 8

For computing the  $n^{\text{th}}$  cumulant of the aggregate interference for interfering picocells in  $\mathcal{R}_2$ , we, once again, begin formulating the corresponding CF as

$$\Psi_{Z_2}(\omega) = \exp \left\{ 2\pi \int_0^\infty \int_{R_m}^{R_M} \left[ \exp(j\omega p r^{-\alpha} x) - 1 \right] \lambda f_X(x) \mathbb{1}_{\Phi^c}^c(p_b r^{-\alpha} x) r dr dx \right\}. \quad (40)$$

where  $\mathbb{1}_{\Phi^c}^c(p_b r^{-\alpha} x)$  corresponds to the event of not detecting interfering picocells.

The  $n^{\text{th}}$  cumulant is then given by

$$\begin{aligned} \kappa_n &= 2\pi\lambda \int_0^\infty \int_{\max[R_m, (x/\varrho_{th})^{1/\alpha}]}^{R_M} p^n r^{1-n\alpha} x^n f_X(x) dr dx \\ &= 2\pi\lambda \left[ \int_0^{\varrho_m} \int_{R_m}^{R_M} p^n r^{1-n\alpha} x^n f_X(x) dr dx + \int_{\varrho_m}^{\varrho_M} \int_{(x/\varrho_{th})^{1/\alpha}}^{R_M} p^n r^{1-n\alpha} x^n f_X(x) dr dx \right]. \end{aligned} \quad (41)$$

Similar to the derivation of (36), we first integrate with respect to  $r$  and obtain

$$\kappa_n = \frac{2\pi\lambda p^n}{n\alpha - 2} \left\{ (R_m^{2-\alpha n} - R_M^{2-\alpha n}) \int_{-\infty}^{\varrho_m} x^n f_X(x) dx + \int_{\varrho_m}^{\varrho_M} \left[ x^{\frac{2}{\alpha}} \varrho_{th}^{n-\frac{2}{\alpha}} - x^n R_M^{2-n\alpha} \right] f_X(x) dx \right\}. \quad (42)$$

And after computing the following partial moment, we obtain the expression (17).

$$\mathbb{E}_X^n[-\infty, \varrho_m] = e^{n\mu + \frac{n^2\sigma^2}{2}} (1 - \mathbb{Q}[\tilde{\varrho}_m - n\sigma]). \quad (43)$$

REFERENCES

- [1] C. Prehofer and C. Bettstetter, "Self-organization in communication networks: principles and design paradigms," *IEEE Commun. Mag.*, vol. 43, no. 7, pp. 78–85, Jul. 2005.
- [2] O. Aliu, A. Imran, M. Imran, and B. Evans, "A survey of self organisation in future cellular networks," *IEEE Commun. Surveys Tuts.*, 2012, IEEE early access articles.
- [3] J. Akhtman and L. Hanzo, "Heterogeneous networking: An enabling paradigm for ubiquitous wireless communications," *Proceedings of the IEEE*, vol. 98, no. 2, pp. 135–138, Feb. 2010.
- [4] I. Güvenç, "Capacity and fairness analysis of heterogeneous networks with range expansion and interference coordination," *IEEE Commun. Lett.*, vol. 15, no. 10, pp. 1084–1087, Oct. 2011.
- [5] S. Mukherjee and I. Güvenç, "Effects of range expansion and interference coordination on capacity and fairness in heterogeneous networks," in *45th Asilomar Conference on Signals, Systems and Computers*, Nov. 2011, pp. 1855–1859.

- [6] D. López-Pérez, X. Chu, and I. Güvenç, “On the expanded region of picocells in heterogeneous networks,” *IEEE J. Sel. Areas Commun.*, vol. 6, no. 3, pp. 281–294, Jun. 2012.
- [7] S. Mukherjee, “Distribution of downlink sinr in heterogeneous cellular networks,” *IEEE J. Sel. Areas Commun.*, vol. 30, no. 3, pp. 575–585, Apr. 2012.
- [8] H.-S. Jo, Y. J. Sang, P. Xia, and J. G. Andrews, “Outage probability for heterogeneous cellular networks with biased cell association,” in *IEEE Globecom*, Houston, TX, USA, Dec. 2011.
- [9] S.-Y. Lien, Y.-Y. Lin, and K.-C. Chen, “Cognitive and game-theoretical radio resource management for autonomous femtocells with qos guarantees,” *IEEE Trans. Wireless Commun.*, vol. 10, no. 7, pp. 2196–2206, Jul. 2011.
- [10] K. Okino, T. Nakayama, C. Yamazaki, H. Sato, and Y. Kusano, “Pico cell range expansion with interference mitigation toward LTE-A heterogeneous networks,” in *ICC Workshops*, Kyoto, Japan, Jun. 2011, pp. 1–5.
- [11] S. Mukherjee, “Downlink sinr distribution in a heterogeneous cellular wireless network with biased cell association,” in *IEEE International Conference on Communications*, Ottawa, Canada, Jun. 2012, pp. 6780–6786.
- [12] A. Baddeley, I. Bárány, R. Schneider, and W. Weil, *Stochastic Geometry*. Springer, 2006.
- [13] J. Andrews, R. Ganti, M. Haenggi, N. Jindal, and S. Weber, “A primer on spatial modeling and analysis in wireless networks,” *IEEE Commun. Mag.*, vol. 48, no. 11, pp. 156–163, Nov. 2010.
- [14] H. Inaltekin, M. Chiang, H. V. Poor, and S. B. Wicker, “On unbounded path-loss models: Effects of singularity on wireless network performance,” *IEEE J. Sel. Areas Commun.*, vol. 27, no. 7, pp. 1078–1092, Sep. 2009.
- [15] G. L. Stüber, *Principles of mobile communication*, 2nd ed. Springer, 2000.
- [16] M.-J. Ho and G. L. Stüber, “Capacity and power control for CDMA microcells,” *ACM Journal on Wireless Networks*, vol. 1, no. 3, pp. 355–363, Oct. 1995.
- [17] M. Abramowitz and I. A. Stegun, *Handbook of Mathematical Functions with Formulas, Graphs, and Mathematical Tables*, 9th ed. Dover, 1965.
- [18] J. F. C. Kingman, *Poisson Processes*. Oxford University Press, 1993.
- [19] D. Stoyan, W. S. Kendall, and J. Mecke, *Stochastic Geometry and Its Applications*, 2nd ed. Wiley-Blackwell, 1995.
- [20] A. Ghasemi and E. S. Sousa, “Interference aggregation in spectrum-sensing cognitive wireless networks,” *IEEE J. Sel. Areas Commun.*, vol. 2, no. 1, pp. 41–56, Feb. 2008.
- [21] S. Resnick, *A Probability Path*. Birkhäuser Boston, 1999.
- [22] J. Wu, N. B. Mehta, and J. Zhang, “A flexible lognormal sum approximation method,” in *Globecom*, St. Louis, MO, 28 Nov.–2 Dec. 2005, pp. 3413–3417.
- [23] K. Dimou, M. Wang, Y. Yang, M. Kazmi, A. Larmo, J. Pettersson, W. Muller, and Y. Timner, “Handover within 3GPP LTE: Design principles and performance,” in *IEEE VTC 2009–Fall*, Anchorage, Alaska, USA, Sep. 2009, pp. 1–5.
- [24] 3GPP, “3G home Node B study item,” TS23.009, version 11.0.0 release 11, Tech. Rep., Sep. 2011.
- [25] —, “Evolved universal terrestrial radio access network X2 application protocol (X2AP),” TS36.423, version 11.2.0 release 11, Tech. Rep., Sep. 2012.
- [26] P. Omiyi, H. Haas, and G. Auer, “Analysis of TDD cellular interference mitigation using busy-bursts,” *IEEE Trans. Wireless Commun.*, vol. 6, no. 7, pp. 2721–2731, Jul. 2007.
- [27] G. T. R. WG4, “Interference mitigation for HeNBs by channel measurements,” Institute for information industry and Colier corporation, TSG-RAN WG4 #52bis, TR, Aug. 2009.

- [28] S. Sesia, I. Toufik, and M. Baker, Eds., *LTE, The UMTS Long Term Evolution: From Theory to Practice*. Wiley, 2009.
- [29] Z. Bharucha, A. Saul, G. Auer, and H. Haas, "Dynamic resource partitioning for downlink femto-to-macro-cell interference avoidance," *EURASIP Journal on Wireless Communications and Networking*, vol. 2010, May 2010.
- [30] 3GPP, "Coordinated multi-point operation for lte," Samsung, TSG-RAN WG1 #53bis, Work Item Description, Sep. 2011.
- [31] J. Zhang and J. G. Andrews, "Adaptive spatial intercell interference cancellation in multicell wireless networks," *IEEE J. Sel. Areas Commun.*, vol. 28, no. 9, pp. 1455–1468, Dec. 2010.
- [32] —, "Distributed antenna systems with randomness," *IEEE Trans. Wireless Commun.*, vol. 8, no. 9, pp. 3636–3646, Sep. 2008.
- [33] C. H. M. de Lima, M. Bennis, and M. Latva-aho, "Coordination mechanisms for self-organizing femtocells in two-tier coexistence scenarios," *IEEE Trans. Wireless Commun.*, vol. 11, no. 6, Jun. 2012.
- [34] M. Dale, *The Algebra of Random Variable*. Wiley & Sons Inc, 1979.
- [35] E. T. Bell, "Exponential polynomials," *The Annals of Mathematics*, vol. 35, no. 2, pp. 258–277, Apr. 1934.
- [36] M. G. Kendall, *The Advanced Theory of Statistics*, 2nd ed. Charles Griffin & Company Limited, 1945, vol. 1.
- [37] S. Weber, J. Andrews, and N. Jindal, "An overview of the transmission capacity of wireless networks," *IEEE Trans. Commun.*, vol. 58, no. 12, pp. 3593–3604, Dec. 2010.
- [38] W. C. Y. Lee, "Estimate of channel capacity in rayleigh fading environment," *IEEE Trans. Veh. Technol.*, vol. 39, no. 3, pp. 187–189, Aug. 1990.
- [39] M.-S. Alouini and A. J. Goldsmith, "Area spectral efficiency of cellular mobile radio systems," *IEEE Trans. Wireless Commun.*, vol. 48, no. 4, pp. 1047–1066, Jul. 1999.

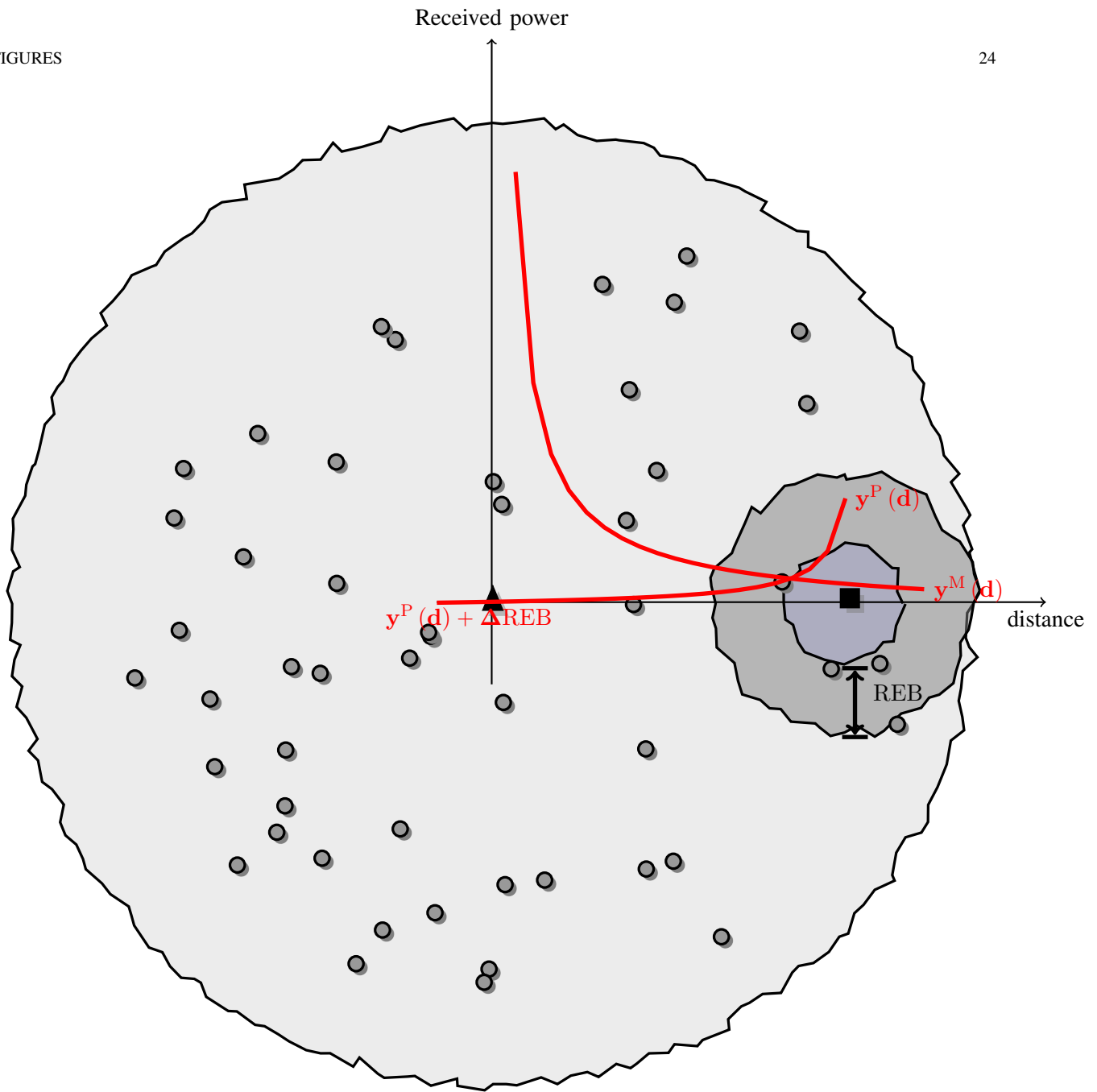


Fig. 1. Illustration of the REB concept. Circles indicate MUs, the shaded triangle depicts the umbrella MBS and the shaded square depicts the target picocell.



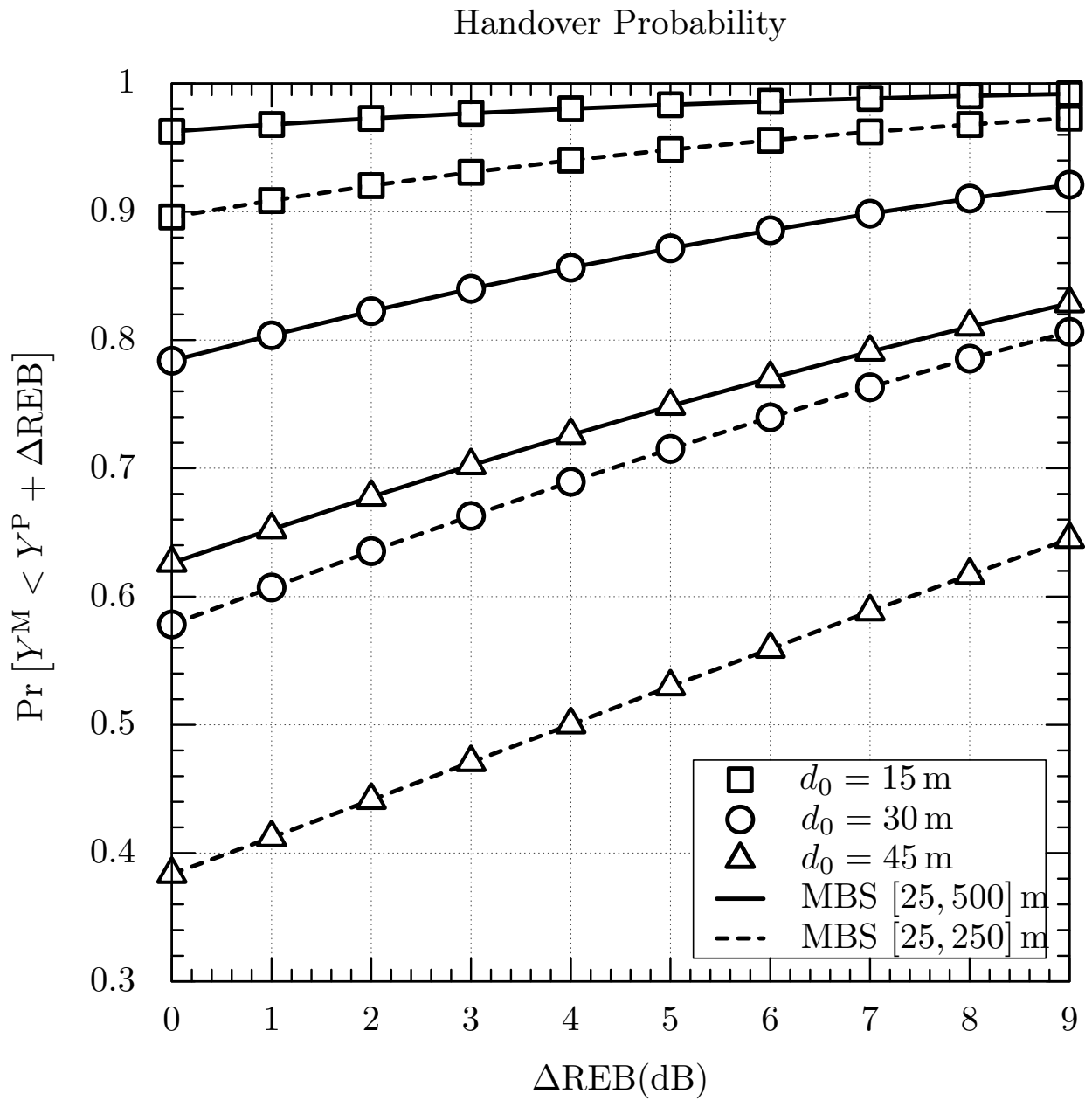


Fig. 2. Handover probability as a function of increasing  $\Delta REB$  values.

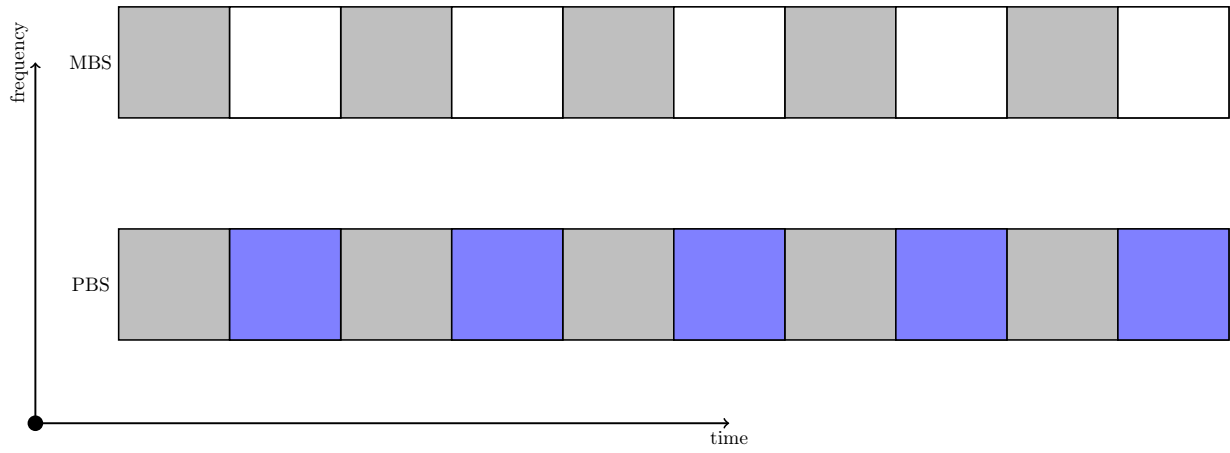


Fig. 3. Illustration of the ABS strategy with rate of  $1/2$ . The umbrella MBS leaves every second subframe (reserved slot) empty so that cell edge MUs which were reassigned to the picocell tier experience less interference.

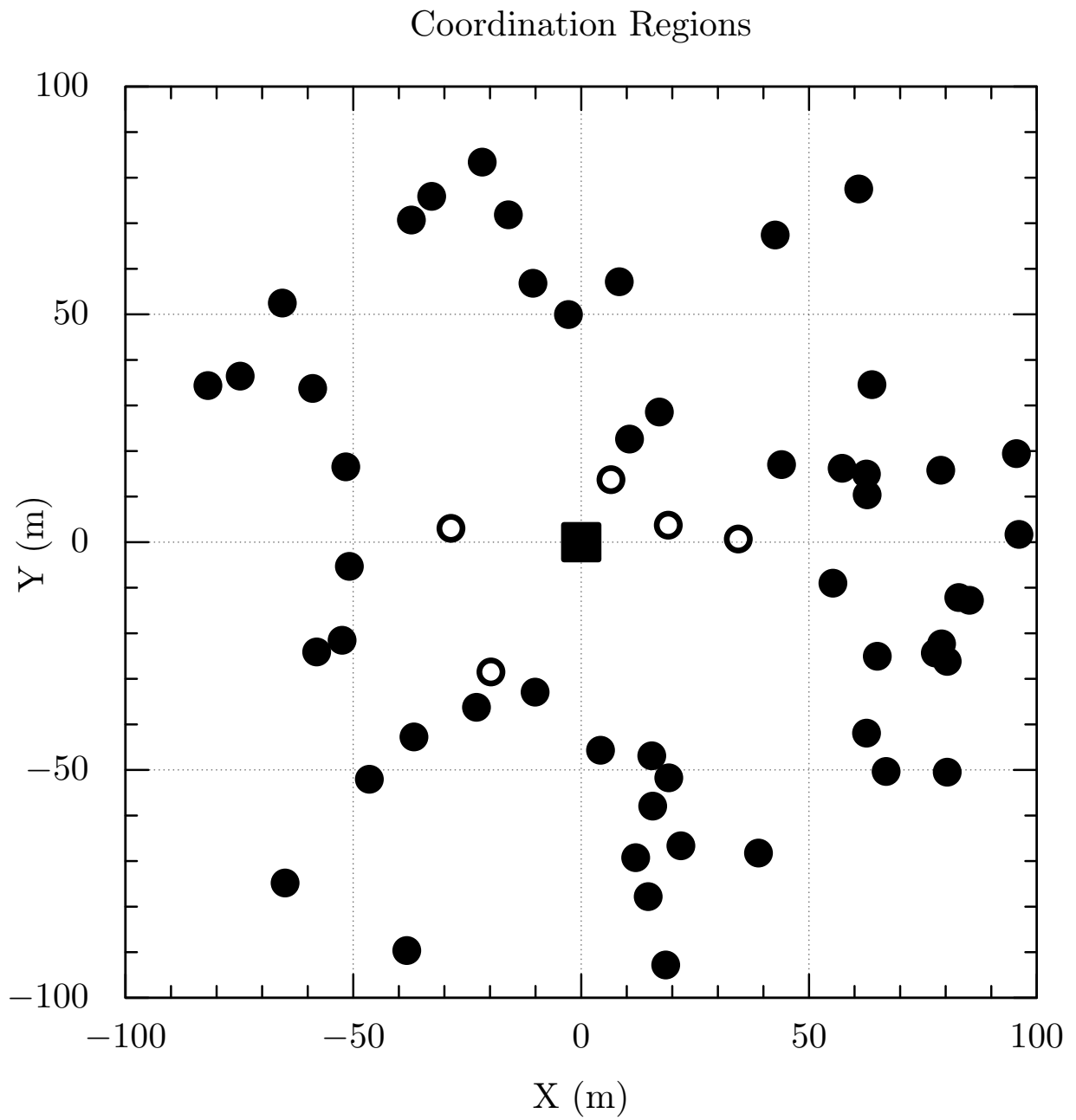


Fig. 4. Illustration of the interfering regions. Unshaded circles identify dominant interferers within  $\mathcal{R}_1$  whose received power is above the threshold predefined  $\rho_{th}$ . Shaded circles identify remaining interferers within  $\mathcal{R}_2$ .

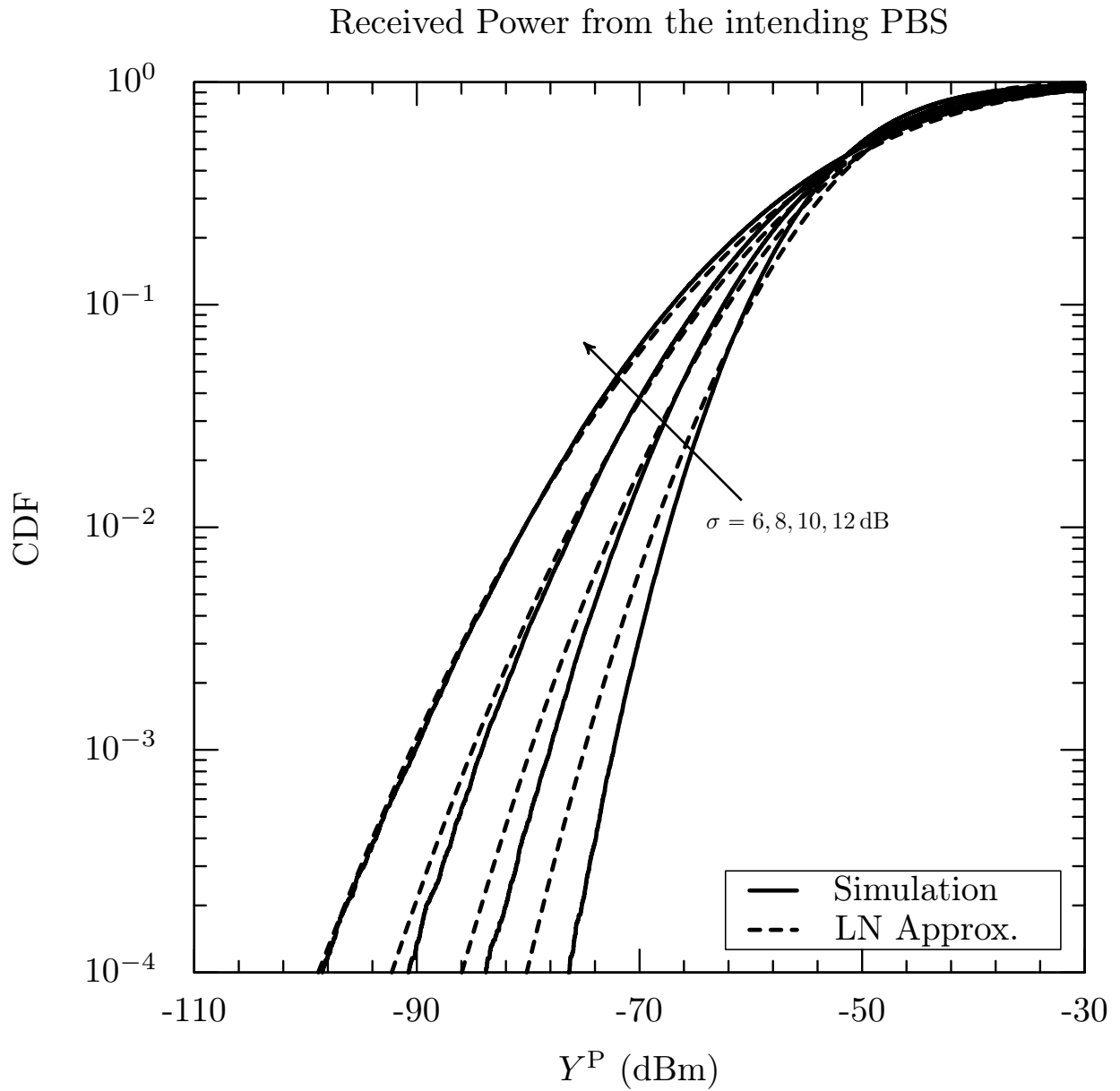


Fig. 5. CDF of the power received by the tagged receiver from a random picocell within its observation region under shadowed fading with  $\sigma = \{6, 8, 10, 12\}$  dB and shape parameter  $m = 16$  (corresponds to a Rician factor  $K = 14.8$  dB). PBSs transmit with constant power equal to 30 dBm.

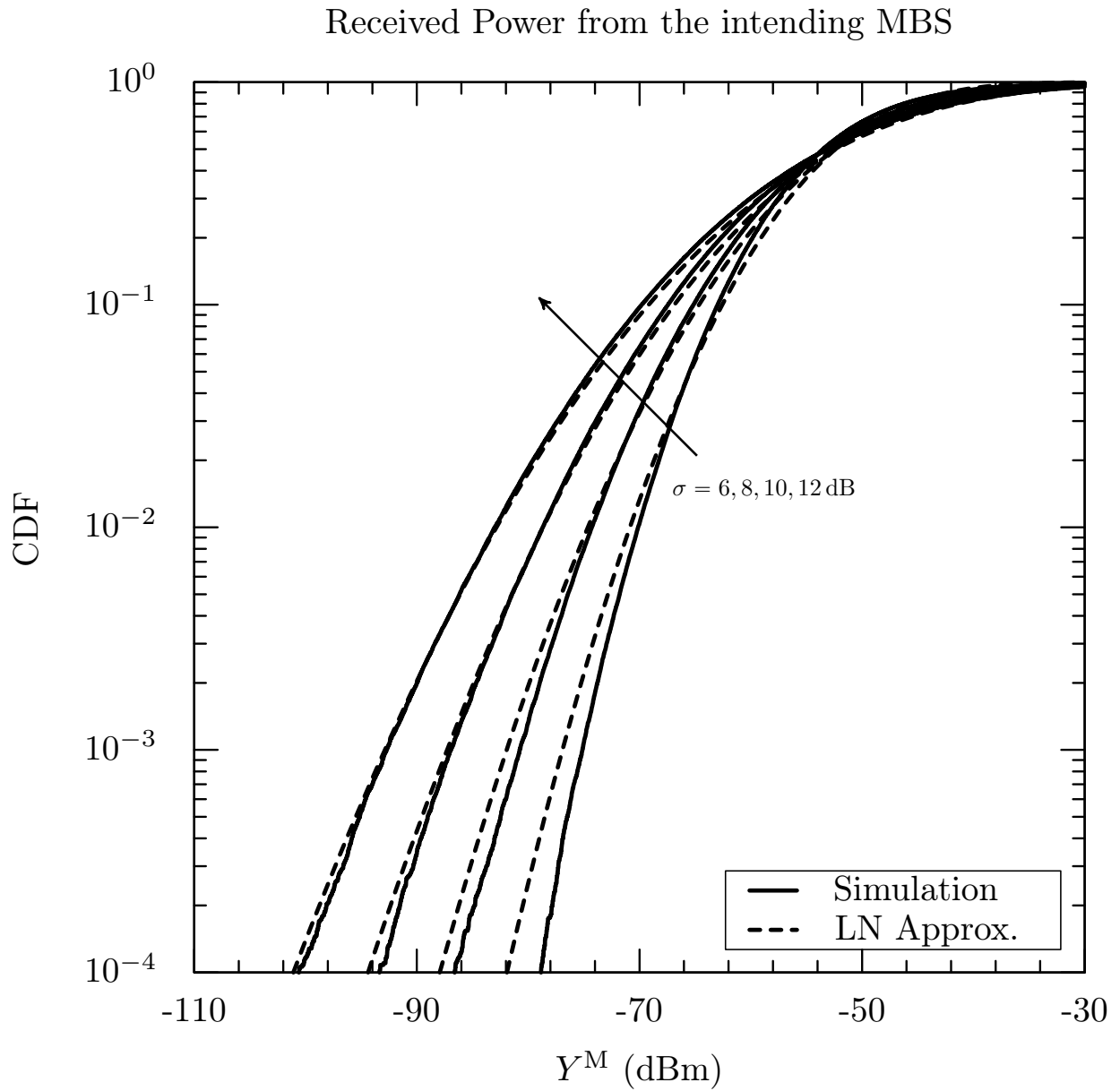


Fig. 6. CDF of the power received by the tagged receiver from a random transmitter within its observation region under shadowed fading with  $\sigma = \{6, 8, 10, 12\}$  dB and shape parameter  $m = 16$  (corresponds to a Rician factor  $K = 14.8$  dB). The umbrella MBSs transmit with constant power equal to 43 dBm, respectively.

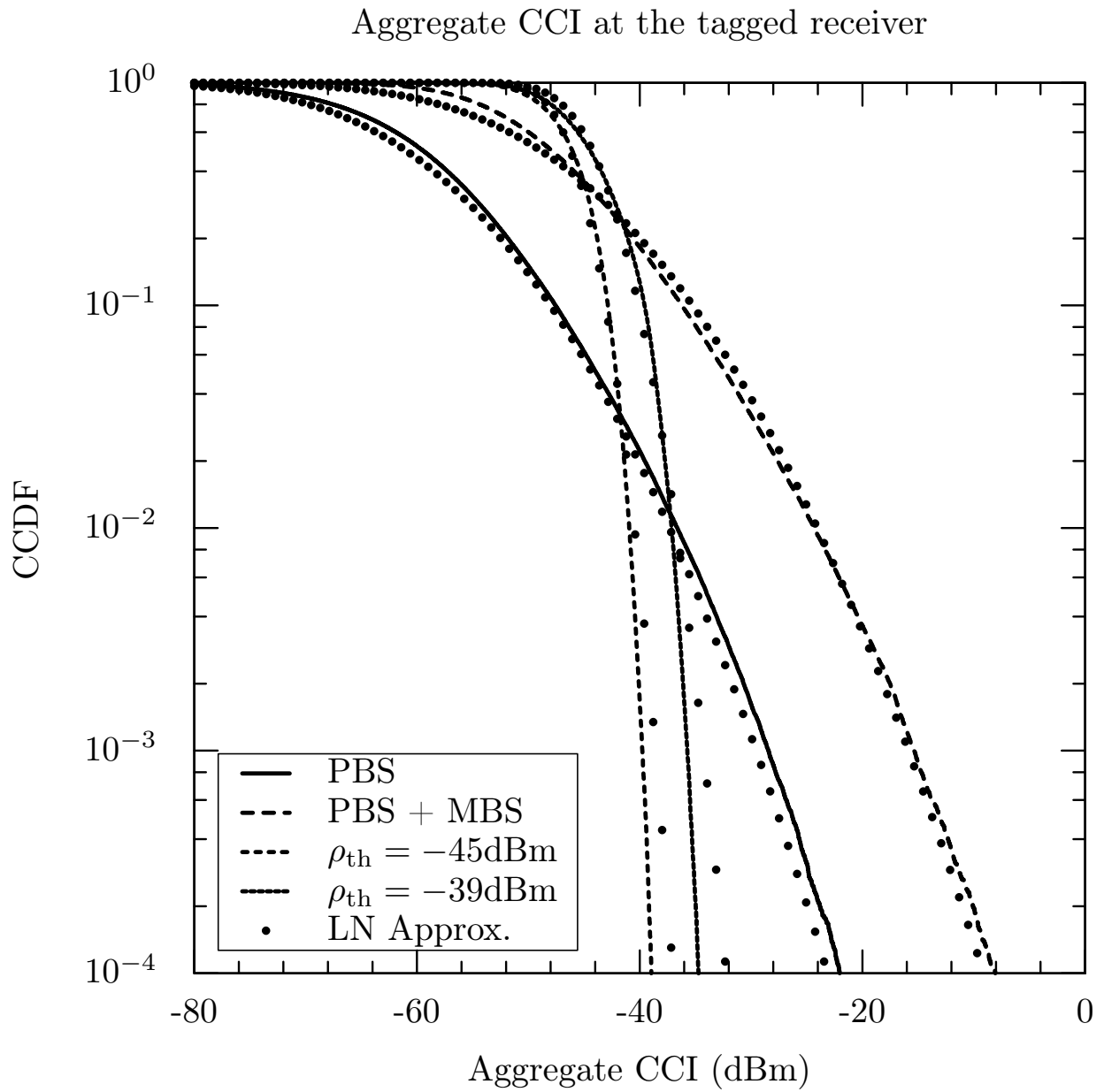


Fig. 7. CCDF of the aggregate CCI  $Z$  at the tagged receiver for the interference scenarios of Section V.

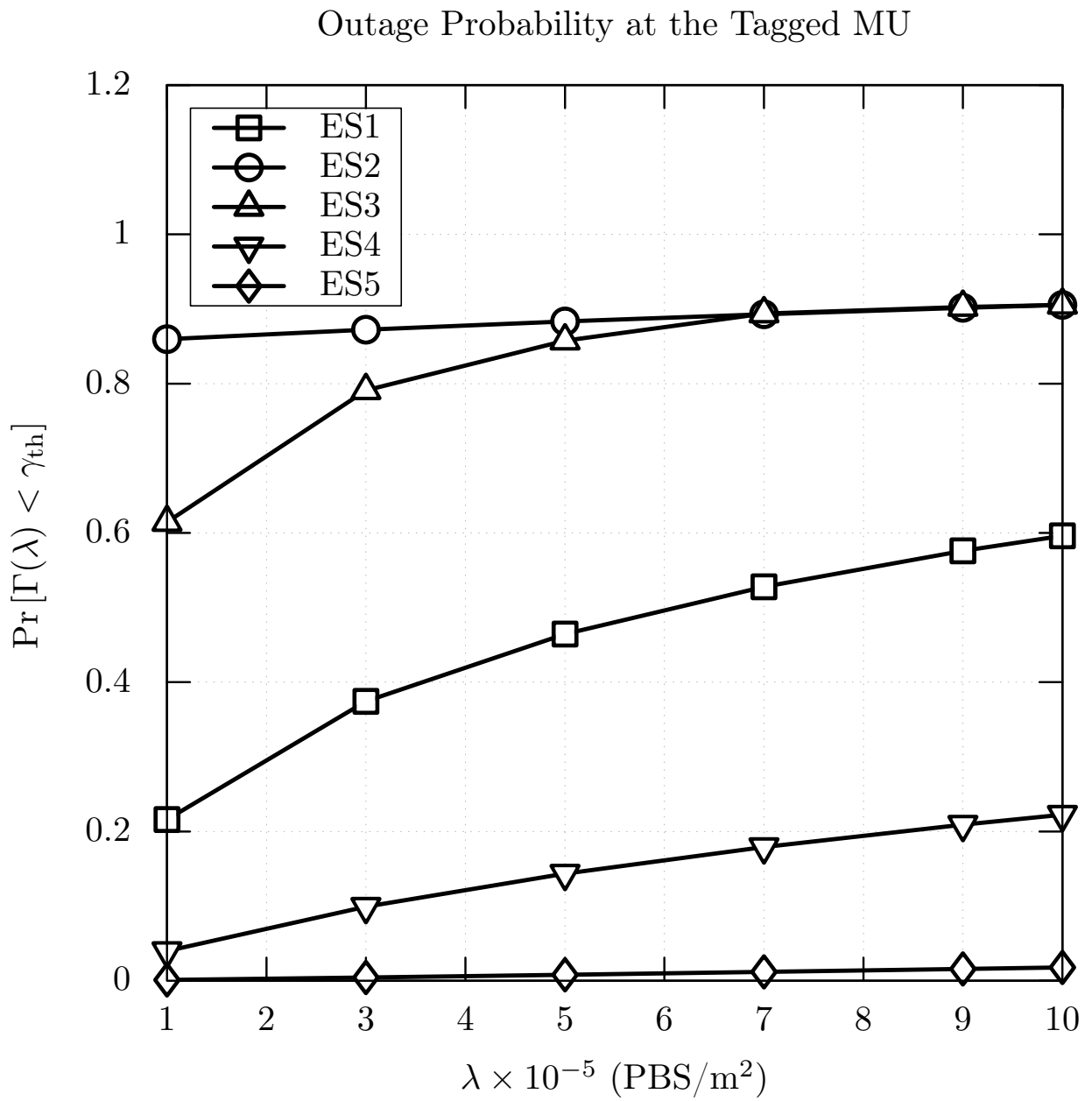


Fig. 8. Outage probability at the tagged receiver for increasing density of interfering picocells.

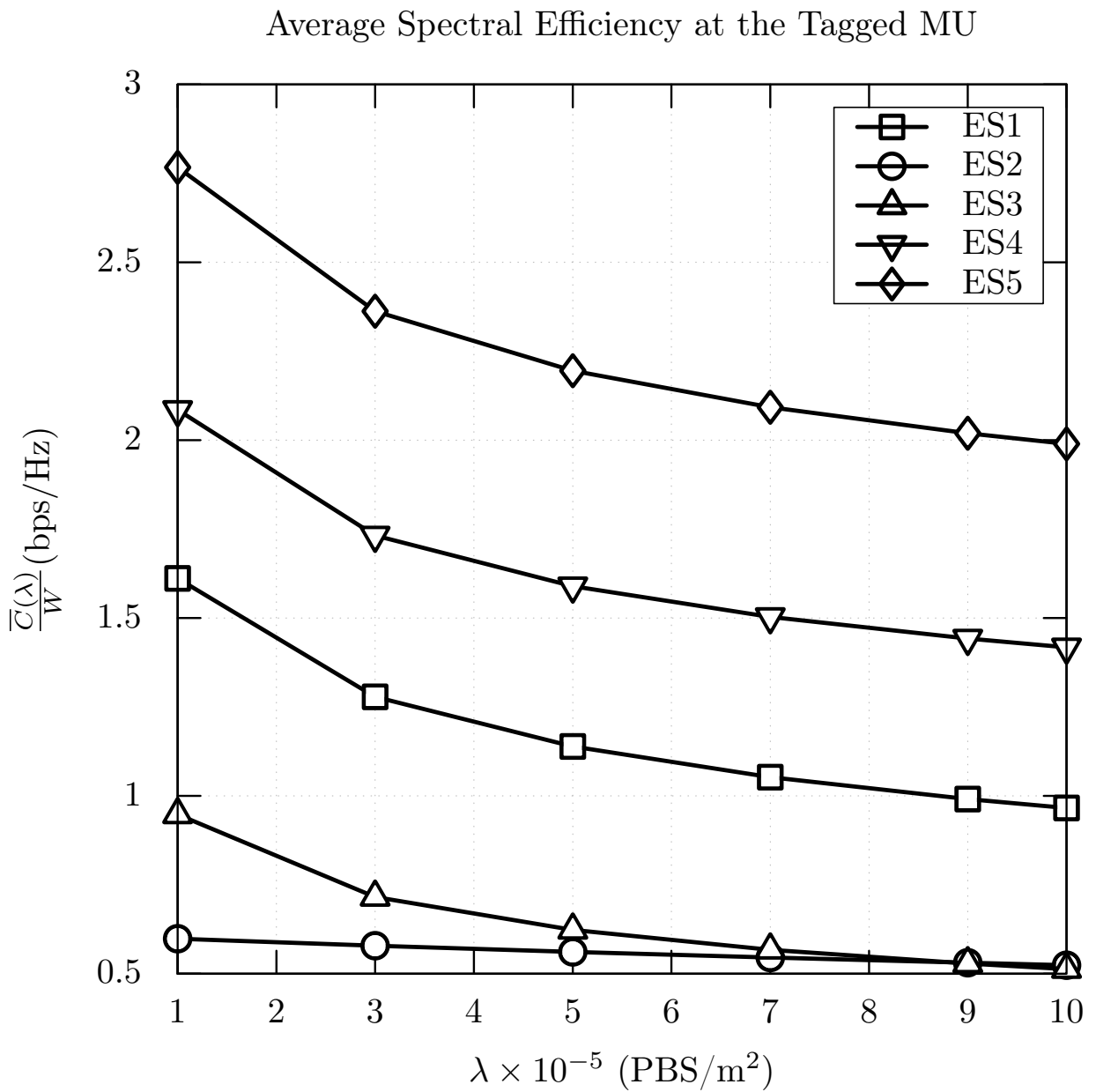


Fig. 9. Average channel capacity at the tagged receiver for increasing density of interfering picocells.